Transferring Rydberg wave packets between islands across the chaotic sea

S. Yoshida,[1] C. O. Reinhold,[2,3] J. Burgdörfer,[1,3] J. J. Mestayer,[4] J. C. Lancaster,[4] and F. B. Dunning[4]
[1]*Institute for Theoretical Physics, Vienna University of Technology, Vienna, Austria*
[2]*Physics Division, Oak Ridge National Laboratory, Oak Ridge, Tennessee 37831-6372, USA*
[3]*Department of Physics, University of Tennessee, Knoxville, Tennessee 37996, USA*
[4]*Department of Physics and Astronomy and the Rice Quantum Institute, Rice University, Houston, Texas 77005-1892, USA*
(Received 22 October 2007; published 25 January 2008)

A protocol to take a Rydberg wave packet that is trapped in a period-1 island, i.e., that is synchronized with the period of the driving field, and transfer it to a period-2 island such that the wave packet evolves with twice the period is theoretically analyzed and experimentally demonstrated. Such period-doubling transitions are realized using two superposed trains of half-cycle pulses whose relative time delay is varied adiabatically. It is shown that this protocol provides a tool to manipulate the angle variable of a Rydberg wave packet while its conjugate principal action is maintained constant.

DOI: 10.1103/PhysRevA.77.013411 PACS number(s): 32.80.Rm, 42.50.Hz

I. INTRODUCTION

The classical phase space of periodically driven systems is generically characterized by a series of stable islands embedded in a chaotic sea [1–4]. While phase flow between islands that are separated by the chaotic sea is classically forbidden, quantum dynamics allows such transfer by way of "dynamical tunneling" [5,6]. In this work we present a *classical* protocol by which the phase space distribution can be efficiently transferred between islands across the chaotic sea without invoking any quantum effects. Key to the protocol is the transient deformation of the phase space by a near-adiabatic modulation of the driving field. We demonstrate, both theoretically and experimentally, the efficiency of this protocol using atoms in high Rydberg states subject to a sequence of half-cycle pulses (HCPs). One prerequisite for the realization of transport between islands is the creation of an initial state that is well localized within a given island. Such states localized in both coordinate and momentum are usually referred to as "wave packets" and have a nearly classical character.

Classically, localization or trapping of phase space density results from the (nearly) impenetrable borders of the islands, the Kolmogorov-Arnold-Moser (KAM) tori for the periodically driven Rydberg atom [1–4]. Quantum mechanically, trapping in an island corresponds to formation of a nondispersive wave packet [7–9] and results from the modification of the Rydberg eigenenergy spectrum by the periodic external perturbation [7,10]. The driving field helps to preserve phase matching between quasieigenstates of the periodically driven system, i.e., the Floquet eigenstates of the period-1 time evolution operator (Floquet operator) [10]. The spectrum of the corresponding quasienergies is, in part, equispaced, which allows for nondispersive wave packets within classical islands of stability. As in the case of the harmonic oscillator, such nondispersive wave packets behave like classical particles and their dynamics can be controlled and manipulated in much the same way as those of a classical particle. In the following, we use the quantum terminology "wave packet" and the classical phase space distribution interchangeably. Due to the modified eigenenergy spectrum, dispersion is slow, and localized wave packets can be maintained for extended periods. Furthermore, for very high Rydberg states ($n \sim 350$) the Heisenberg (or quantum break) time [1,2] becomes quite large (of the order of microseconds). Within the experimentally accessible observation time ($\sim 1\ \mu$s), quantum and classical dynamics should thus closely mirror each other.

Several protocols to manipulate nondispersive wave packets based on their underlying classical dynamics have been suggested [11–13]. For the periodically kicked Rydberg atom studied in this work, this is accomplished by adiabatically changing the position of the classical resonances at the centers of the stable islands that provide the skeleton for creation of nondispersive wave packets. For weak fields, the largest island occurs when the frequency of the unperturbed electron Kepler orbit $\nu_n = 1/(2\pi n^3)$ (atomic units are used throughout) is synchronized with the frequency ν of the external driving ($\nu \sim \nu_n$). This period-1 island is remarkably robust against slow changes in the external driving field and is therefore the preferred starting point for steering Rydberg wave packets to different regions of phase space by adiabatically modulating (chirping) the period or the strength of the driving field [12,14].

In this work we describe a technique for transferring a wave packet from this period-1 island to a pair of period-2 islands across the chaotic sea. This is accomplished by taking advantage of a protocol that employs two superposed trains of identical pulses, each with the same period, whose relative time shift τ is adiabatically varied. A notable feature of such time shift chirping is that it is possible to keep the principal action n (approximately) constant while slowly changing the stroboscopic value of the conjugate angle variable, the "mean anomaly" θ [15]. In contrast, simply chirping the period of a train of pulses leads to the opposite result, i.e., the action is changed while the angle remains approximately constant. The two chirping protocols thus complement each other and provide powerful tools with which to control Rydberg wave packets. The physical processes underlying the present protocol are discussed with the aid of theoretical simulations. To demonstrate the full capabilities of the technique these are undertaken starting with an optimal mix of

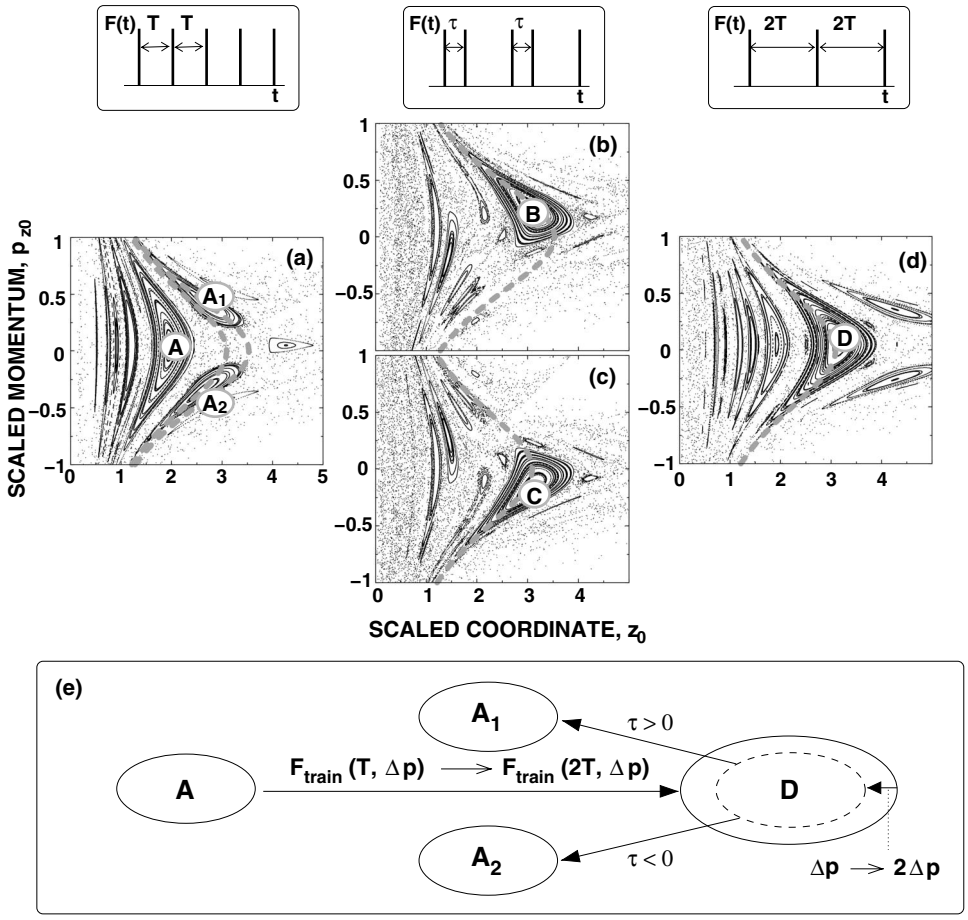

FIG. 1. (a)–(d) Poincaré surfaces of section of the periodically kicked Rydberg atom. (a) A single train is applied with a scaled kick strength of $\Delta p_0 = n_i^4 \Delta p = -0.1$ and period $T = 6$ ns. The stroboscopic snapshots are taken immediately before each kick using a cut at $(\rho, p_\rho) = (0,0)$. (b), (c) Two identical HCP trains with $\Delta p_0 = -0.1$ and period $T' = 12$ ns and a relative time delay $\tau = 3$ ns are applied. The stroboscopic snapshots are taken immediately before each kick in the first (b) and second (c) train. (d) Same as (a) but for a period $T' = 12$ ns. The phase space coordinates are scaled to $n_i = 350$, i.e., $z_0 = z/n_i^2$ and $p_{z0} = p_z n_i$. The upper panels show the associated pulse profiles and each HCP is approximated by a δ function. The gray dashed lines in (a) show Kepler orbits with principal actions of $n_{A_1} \simeq 435$ and $n_{A_2} \simeq 465$. In (b) the Kepler orbit with $n = n_{A_2}$ and in (c) and (d) that with $n = n_{A_1}$ is drawn. In (e), the steps involved in the protocol for transporting phase space density from island A to A_1 or A_2 via D are schematically indicated.

initial states, namely a mix of highly oriented extreme parabolic Stark states. The method is also demonstrated experimentally using a mix of partially oriented Stark states.

II. RYDBERG ATOMS SUBJECT TO PERIODIC PULSES

A. Response to a single periodic train of pulses

The response of a Rydberg atom to a periodic train of N identical half-cycle pulses with profile $F_{\mathrm{HCP}}(t)$ directed along the z axis is governed by the Hamiltonian

$$H(t) = \frac{p^2}{2} - \frac{1}{r} + zF_{\mathrm{train}}(T, \Delta p, t), \tag{1}$$

where $\vec{r} = (x, y, z)$ and $\vec{p} = (p_x, p_y, p_z)$ are the position and momentum of the Rydberg electron, and

$$\begin{aligned} F_{\mathrm{train}}(T, \Delta p, t) &= \sum_{j=1}^{N} F_{\mathrm{HCP}}(t - t_j) \\ &= \sum_{j=1}^{N} F_{\mathrm{HCP}}(t - jT) \\ &\simeq -\sum_{j=1}^{N} \Delta p\, \delta(t - t_j), \end{aligned} \tag{2}$$

$T = t_{j+1} - t_j$ being the period of the train. When the duration of each HCP is much shorter than the electron orbital period, $T_n = 2\pi n^3$ (~ 7–14 ns for the $n = 350$–450 Rydberg states studied here), each HCP simply delivers an impulsive momentum transfer or "kick," $\Delta p = -\int F_{\mathrm{HCP}}(t)dt$, to the excited electron. Here we consider quasi-one-dimensional (quasi-1D) Rydberg atoms oriented along the z axis subject to kicks directed toward the nucleus, i.e., with $\Delta p < 0$.

Figures 1(a) and 1(d) display typical phase space portraits

[Poincaré surfaces of section (PSSs)] for the "kicked" atom when driven by trains of HCPs with periods $T=6$ ns and $T'=12$ ns, respectively, each pulse delivering kicks of scaled strength $\Delta p_0=n_i\Delta p=-0.1$. These portraits exhibit a mixed phase space consisting of stable islands embedded in a chaotic sea. The stroboscopic snapshots used in generating these figures were taken immediately before each kick. Since we focus here on quasi-1D motion along the z axis, the cuts used are for the limit $\rho=\sqrt{x^2+y^2}\to 0$ and $p_\rho=(xp_x+yp_y)/\rho\to 0$. The axes are labeled in scaled units $z_0=z/n_i^2$ and $p_{z0}=p_z n_i$, where $n_i=350$. The stable islands are associated with electron motion that is synchronous with the periodic train leading to dynamical stabilization. Otherwise the electron follows a chaotic trajectory and eventually becomes ionized [4]. Immediately before each kick, the largest islands in Figs. 1(a) and 1(d) are centered, respectively, at $(z0,pz0)\sim(2,-\Delta p0/2)$ (labeled as A) and $(z_0,p_{z0})\sim(3.3,-\Delta p_0/2)$ (labeled as D). Thus the effect of a kick of magnitude $|\Delta p_0|$ in the $-z$ direction on an electron located near the center of either island is to change its z component of momentum from $p_{z0}=+|\Delta p_0|/2$ to $p_{z0}=-|\Delta p_0|/2$, i.e., the z component of its momentum is reversed while its energy remains essentially unchanged. Thereafter, the electron trajectory evolves following an unperturbed Kepler orbit with principal action $n=n_i\sim 350$ [Fig. 1(a)] or $n\simeq 435$ [Fig. 1(d)] until, after a time comparable to a Kepler period, the electron returns to its original position with $p_{z0}=+|\Delta p_0|/2$ and the process repeats. Clearly, synchronization of the kick frequency ν and the Kepler frequency ν_n is a prerequisite for the formation of a stable island. When the period of the pulse train is doubled from $T=6$ ns in Fig. 1(a) to $T'=12$ ns in Fig. 1(d), i.e., when the frequency is reduced by a factor of 2, the center of the island moves away from the nucleus toward larger z because only a smaller Kepler frequency $\sim 1/(2\pi n^3)$ (or larger n) meets the synchronization condition $\nu\sim\nu_n$.

At the higher driving frequency two stable islands [labeled as A_1 and A_2 in Fig. 1(a)] also appear. These are associated with Kepler orbits of higher n than for island A ($n_{A_1}=435$, $n_{A_2}=465$) and are termed period-2 islands. If an electron is located in the island A_1, its momentum is positive $p_z>0$. Therefore, a kick toward the nucleus $\Delta p<0$ decelerates the electron and its energy is reduced. After half a Kepler period, $T\simeq T_{n_{A_1}}/2\sim 6$ ns, the electron reaches the island A_2 with negative momentum $p_z<0$. Application of another kick ($\Delta p<0$) at this time accelerates the electron and the energy is increased. The losses and gains in energy following successive kicks cancel and the net energy transfer vanishes. The electron transitions periodically between Kepler orbits with $n\sim 435$ and 465. Since the composite orbit returns the electron to island A_1 or A_2 only after every other kick, it is called a period-2 orbit. The dynamics of period-2 islands are more complex than those of period-1 islands such as A or D. In consequence, they are less stable, as evidenced in the PSSs by the smaller areas covered by island A_1 or A_2 as compared to island A or D. It is thus more challenging to trap a wave packet in period-2 islands. Once a wave packet is loaded, however, its evolution can be rather easily monitored using a probe HCP because the centers of the islands A_1 and A_2 correspond to opposite signs of p_z. For a probe kick directed along, say, the $+z$ axis, a wave packet positioned in island A_1 ($p_z>0$) will gain energy, leading to ionization, whereas a wave packet positioned in island A_2 ($p_z<0$) will lose energy, and little ionization will occur. The resulting changes in survival probability as the wave packet oscillates between A_1 and A_2 thus provide a clear signature of the population of period-2 islands. Furthermore, once the train of HCPs is turned off the wave packet will evolve at a rate characteristic of the period of the final n manifold. Since the period-2 orbit involves two different energy manifolds [the two dashed lines shown in Fig. 1(a)] the periodic transitions between A_1 and A_2 can be seen by monitoring the time evolution of the final state using a probe HCP applied after a variable time delay [8].

B. Response to a superposition of two trains of pulses: Transfer between islands

The main objective of the present work is to establish a protocol to transfer an electron wave packet from the period-1 island centered at A to the period-2 islands centered at A_1 and A_2, all of which are islands of stability for the "same" train of pulses (e.g., with the same kick strength $\Delta p_0=-0.1$ and period $T=6$ ns). Previously, protocols have been devised to navigate wave packets in phase space by adiabatically chirping the period (frequency) and/or the strength of pulses in a train. For example, transport of a wave packet located in the island centered at A [Fig. 1(a)] to a location near the island centered at D [Fig. 1(d)] can be accomplished by adiabatically chirping the interval $t_{j+1}-t_j$ between successive HCPs in the train from $T=6$ ns to $T'=2T=12$ ns, i.e., by a negative frequency chirp,

$$F_{\text{train}}(T,\Delta p,t)\to F_{\text{train}}(T'=2T,\Delta p,t). \tag{3}$$

However, any adiabatic modulation of a single train of pulses that starts and ends with the same train, i.e., the same values of T and Δp, will return the wave packet to its original location in phase space. Transfer from a period-1 to a period-2 island thus requires the introduction of a new control variable, which we obtain by superposing a second train of pulses.

To understand the protocol, it is instructive to first analyze the phase space structure for a Rydberg atom subject to the following superposition F_s of two identical pulse trains each of which is periodic with period T':

$$F_s(T',\Delta p,\tau,t)=F_{\text{train}}(T',\Delta p,t)+F_{\text{train}}(T',\Delta p,t-\tau), \tag{4}$$

where τ is the relative time shift between the trains. This superposition is also periodic in time with period T' and contains two pulses per period. Correspondingly, the phase space portrait evolves periodically in time. Figures 1(b) and 1(c), respectively, show PSSs immediately before each kick in the first train at times $t=jT'$ and before each kick in the second train at times $t=jT'+\tau$ for $\tau=3$ ns. During the time interval τ the Poincaré surface of section changes from that in Fig. 1(b) to that in Fig. 1(c) before returning to that in Fig. 1(b) a time $2T-\tau$ later.

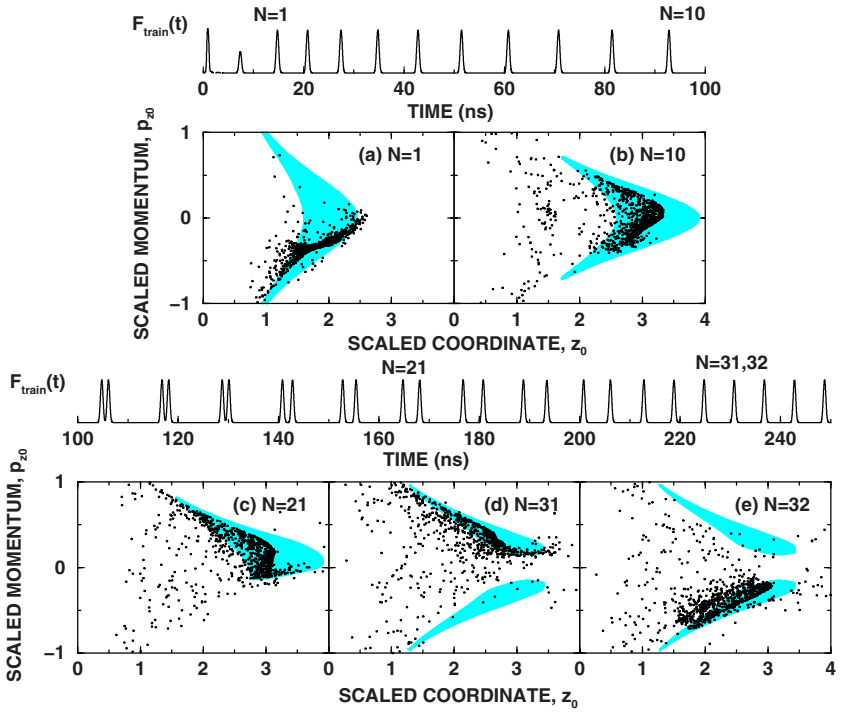

FIG. 2. (Color online) Calculated evolution of the phase space distribution of the wave packet for an initial mix of maximally polarized Stark states (see text). The phase space distributions are projected on the (z,p_z) plane and are taken at the times when the 1st, 10th, 21st, 31st, and 32nd HCPs reach their peak values. The shaded areas represent the stable islands associated with the transient train of pulses in which the wave packet is evolving. The colored line shows the profile of the applied HCP sequence.

The present protocol is based on the fact that the superposition in Eq. (4) has the following limits:

$$F_s(T',\Delta p,\tau \to 0,t) = F_{\text{train}}(T',2\Delta p,t), \tag{5}$$

$$F_s(T',\Delta p,\tau \to T,t) = F_{\text{train}}(T,\Delta p,t). \tag{6}$$

As $\tau \to 0$, F_s collapses to a single train of pulses of period $T'=2T=12$ ns as used to generate Fig. 1(d) but with twice the amplitude $(2\Delta p)$. However, this leads to little change in the PSS because Δp is small. The size of the island D is slightly reduced but its position is largely unchanged. Conversely, as $\tau \to T=T'/2$ we recover a pulse train identical to that used to generate Fig. 1(a). As τ is varied from 0 to T, the period-1 island D is thus "morphed" into the period-2 islands A_1 and A_2 through the intermediate island structure shown in Figs. 1(b) and 1(c), i.e., through the islands labeled B and C. Therefore, as illustrated schematically in Fig. 1, by chirping the frequency of the HCP train [Eq. (3)], introducing a second superposed HCP train [Eq. (4)] and varying the time delay τ, a wave packet initially localized in the period-1 island A can be adiabatically transferred to the period-2 islands A_1 and A_2. A diagram of the path followed by the wave packet is shown in Fig. 1(e). Using the control knob τ we can form a closed loop that ends with the initial HCP train without returning the wave packet to its initial location. Instead, we transfer the phase space distribution from one island to another.

The HCP sequence used in the present protocol is shown in Fig. 2 and consists of the following elements that can be realized experimentally.

(1) Starting from a mix of quasi-1D $n_i=350$ Stark states a transiently localized wave packet is prepared and loaded into island A, as described in detail elsewhere [16], using the two weak localization kicks. The first has a scaled strength of $\Delta p_{0L}=-0.085$. The second is applied after a 6.5 ns delay and is of strength $\Delta p_{0T}=-0.05$.

(2) The main HCP train begins 7.4 ns later and has a scaled strength of $\Delta p_0=-0.1$. The period of this train is incremented over the ten pulses labeled $N=1-10$ according to $t_{N+1}-t_N=T+\delta T(N-1)$, where $T=6$ ns and $\delta T=0.67$ ns. That is, the period is linearly increased from $T=6$ ns to $T'=12$ ns in increments of 0.67 ns (set by experimental considerations). This transfers the wave packet from island A (with $n_i \sim 350$) to island D with $n \sim n_{A_1} \sim 435$.

(3) A second identical periodic train of HCPs with period $T'=12$ ns is then superposed with an initial relative time shift $\tau=2\delta T=1.3$ ns. (Given that this separation is short compared to the electron orbital period, their combined effect is similar to that of a single pulse of twice the strength. However, as noted previously, this leads to only small changes in the position and shape of island D.) The time shift and period of these trains are kept constant for three periods, i.e., for the six pulses extending from $N=11$ to 16.

(4) The wave packet is then transferred from island D to the period-2 islands A_1 and A_2 by linearly increasing the time shift τ from 1.3 to 6 ns, again in increments of $\delta T=0.67$ ns, over the next 12 pulses $N=17-29$. That is, kicks $N=17-28$ are applied at times $t_N=t_{15}+T(N-15)$ for N odd and $t_N=t_{N-1}+2\delta T+(\delta T/2)(N-16)$ for N even.

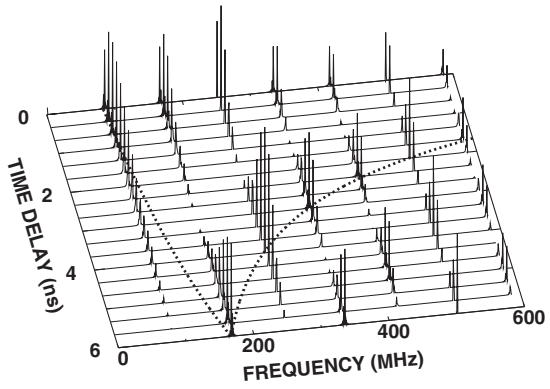

FIG. 3. Power spectrum of the pulse train F_s [Eq. (7)] as a function of the time delay τ separating the two trains of HCPs. Each HCP has a pulse duration of 600 ps at full width at half maximum, $\Delta p_0 = -0.1$, and period $T' = 2T = 12$ ns.

(5) Finally, for pulses $N = 30, 31, \ldots$ the train is held fixed (with period $T = 6$ ns) to maintain the product wave packet in the period-2 islands.

In order to understand the dynamical implications of varying the time delay τ between the superposed trains [Eq. (4)] we analyze the parametric variation of the power spectrum of F_s, given by

$$\tilde{F}_s(T', \Delta p, \tau, \nu) = \left| \int [F_s(2T, \Delta p, \tau, t) - \langle F_s \rangle] e^{2\pi\nu t} dt \right|^2, \tag{7}$$

as a function of τ. This is shown in Fig. 3 for HCP widths of 600 ps with the average (zero-frequency component) subtracted. For $\tau = T = 6$ ns, the spectrum features the fundamental frequency $\nu = 1/T = 166$ MHz plus a range of higher harmonics with slowly decaying amplitude. As τ is reduced from $\tau = T$ to $\tau = 0$ the frequency spectrum "branches" (as indicated by the two dashed lines), developing a strong high-frequency component ($\nu \sim 1/\tau$) as well as a period-doubled low-frequency component at $\nu' = 1/T' = 83$ MHz. The high-frequency component in the power spectrum for small τ raises the possibility that classical-quantum correspondence might break down. Classically, the energy gain by an electron due to a high frequency ($\nu_\tau \sim 1/\tau$) monochromatic field $F_0 \cos(2\pi\nu_\tau t)$ can be written as $\Delta E(t) = \int dt\, z(t) F_0 \cos(2\pi\nu_\tau t)$. Far from the nucleus the electron moves slowly and its position $z(t)$ remains essentially constant over a period of the (high-frequency) field leading to negligible energy transfer. In contrast, near the nucleus $z(t)$ changes rapidly, allowing finite energy transfer (gain or loss) to the electron. Quantum mechanically, the strong acceleration near the nucleus in the presence of strong high-frequency fields leads to the absorption (or emission) of photons, leading to above-threshold ionization or high harmonic generation [17]. However, while the HCP train contains many high-frequency components, it can excite the electron only in the 600 ps intervals during which each HCP is applied. As illustrated by islands B and C in Figs. 1(b) and 1(c), at such times the wave packets of interest here are localized far from the nucleus. Therefore, near the nucleus electrons experience only the Coulomb force, whereupon photoexcitation and photoionization are suppressed (numerically it can be shown that dipole matrix elements involving a wave packet localized near the outer turning point are small [18], indicating that photoexcitation or -ionization takes place mainly near the nucleus). Classical-quantum correspondence is thus well preserved even though high-frequency components are present in the driving field.

III. SIMULATION FOR MAXIMALLY POLARIZED STATES

Figure 2 displays the results of classical trajectory Monte Carlo (CTMC) simulations that show the time evolution of the wave packet during the HCP sequence outlined above. The initial state is represented by a restricted microcanonical ensemble of phase points that encompasses a mix of the 18 extreme redshifted states in the $n_i = 350$, $m = 0$ Stark manifold, i.e., the states with values of the electric quantum number $k = -n_i + 1, \ldots, -n_i + 35$. Because stable islands of the periodically kicked atom are observed only along the z axis ($\rho \simeq 0$), this choice of initial states maximizes the overlap between the initial wave packet and the target stable island, optimizing the trapping efficiency. The number of parabolic states included in the initial distribution is chosen according to the effective laser linewidth (see Sec. IV). However, the precise number is not important as long as the width of the wave packet does not exceed the transverse dimension of the stable island. The time evolution of the wave packet (i.e., of the distribution of associated phase points) is followed by solving the Hamilton equations of motion for each initial phase space point. (All CTMC simulations of wave packet evolution employ the experimentally measured HCP profiles rather than δ-function kicks.) After application of the loading pulses the wave packet is localized (transiently) [16] in the initial period-1 island [Fig. 2(a)], where it remains trapped as the HCP frequency is chirped to transfer the wave packet to states with $n \sim n_{A_1} \sim 435$ [Fig. 2(b)]. After introduction of the second HCP train, the wave packet remains trapped in island D and follows its evolution as the time shift τ is increased [Fig. 2(c)]. When τ reaches 6 ns and the train becomes periodic and the wave packet is trapped in the period-2 islands, hopping between them at each kick [Figs. 2(d) and 2(e)].

The final trapped wave packet can be examined using a probe HCP that is applied at a preselected time delay τ_{delay} following the last HCP pulse in the train. A probe HCP with strength Δp_{probe} transfers an energy $\Delta E = p_z \Delta p_{\text{probe}} + (\Delta p_{\text{probe}})^2/2$ to the electron. If the final wave packet lies near the n_{A_1} manifold, the atom will be ionized when ΔE exceeds the ionization potential $I_{n_{A_1}} = 1/(2n_{A_1}^2)$. That part of the wave packet residing in the region where $p_z > I_{n_{A_1}}/(\Delta p_{\text{probe}}) - \Delta p_{\text{probe}}/2$ is therefore ionized. Thus, measurements of the survival probability as Δp_{probe} is varied provide information on the momentum distribution of the product wave packet [19]. This is illustrated in Fig. 4(a), which shows calculated survival probabilities as a function of Δp_{probe} for a probe pulse applied 6 ns after the $N = 31$ and 32

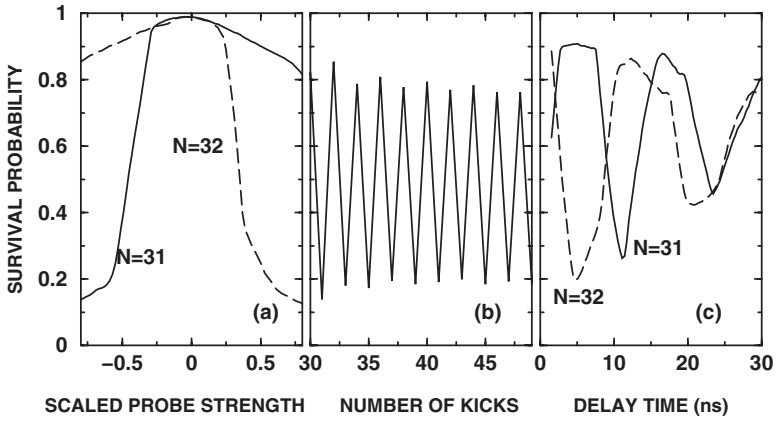

FIG. 4. Dependence of the calculated survival probabilities on (a) the strength and direction of the probe kicks, (b) the number of kicks N in the HCP train, and (c) the delay time τ_{delay} between the end of the HCP train and application of the probe kick. In (a) the probe HCP is applied 6 ns after the 31st (solid) and the 32nd (dashed) kicks. In (b) the train of HCPs is turned off after N kicks and the probe HCP with strength $\Delta p_{\text{probe},0}=-0.8$ is applied 6 ns later. In (c) the probe HCP $\Delta p_{\text{probe},0}=0.5$ is applied after the 31st (solid) and 32nd (dashed) kicks. The initial wave packet is taken to be a mix of the 18 extreme redshifted Stark states in the $n_i=350$, $m=0$ manifold and is oriented along the same axis as the applied HCPs.

kicks. Following the 31st kick, the wave packet is positioned within island A_1 having $p_z>0$ [Fig. 2(d)] and evolves toward island A_2 ($p_z<0$) during the 6 ns delay. A negative probe pulse $\Delta p_{\text{probe}}<0$ therefore accelerates the electron, leading to large ionization probabilities. In contrast, for $\Delta p_{\text{probe}}>0$ the electron loses energy, greatly reducing the likelihood of ionization. The sudden fall-off in the survival probability around $\Delta p_{\text{probe},0}=-0.5$ points to strong wave packet localization. Following $N=32$ kicks, the survival probability is almost a mirror image of that for $N=31$ kicks, demonstrating that the wave packet is localized within island A_2 having $p_z<0$.

Beyond $|\Delta p_{\text{probe},0}|=0.5$, the difference between the survival probabilities following $N=31$ and 32 kicks becomes quite large (the difference is ~70%). This large contrast provides a signature that can be used to examine just how long a wave packet can be kept trapped inside the period-2 islands. This is illustrated in Fig. 4(b) for a fixed scaled probe kick strength $\Delta p_{\text{probe},0}=-0.8$ and a fixed delay time $\tau_{\text{delay}}=6$ ns. The survival probability is calculated as a function of the number of kicks prior to the probe and mirrors the dynamical behavior of the average momentum $\langle p_z(t)\rangle$ of the wave packet during the HCP sequence. As shown in Fig. 4(b), even after 50 kicks, the survival probability alternates between values of 0.2 and 0.8, indicating that the wave packet is well trapped within the period-2 island.

As noted previously, the period-2 orbit involves two different energy manifolds n_{A_1} and n_{A_2} ($>n_{A_1}$). This energy difference can be examined using a probe HCP of fixed strength applied after different time delays following the last HCP in the train. Once the HCP train is turned off, the wave packet evolves freely and the resulting survival probability exhibits periodic behavior with period $T_n=2\pi n^3$ that is characteristic of the average principal action n of the final wave packet. Thus the periodic variations in survival probability can be mapped onto the average principal action prior to the 31st kick [Fig. 2(d)]; the wave packet is located in island A_1 with $p_z>0$. During the HCP the wave packet is decelerated and then follows the Kepler orbit with the smaller energy $n=n_{A_1}$. In contrast, after the 32nd kick, the wave packet is returned to the higher-energy manifold $n=n_{A_2}$. Therefore the time evolution of the wave packet, i.e., of the survival probability [Fig. 4(c)], following $N=31$ kicks is somewhat faster than that after $N=32$ kicks. The oscillation periods of approximately 12.5 and 15.3 ns correspond to population of states with $n_{A_1}\simeq 435$ and $n_{A_2}\simeq 466$.

The current protocol has the remarkable additional feature that it allows control of the stroboscopic value of the canonical angle θ, the so-called mean anomaly (i.e., the conjugate angle of the principal action n). Prior to the superposition of the second HCP train [Eq. (4)] the periodic orbit at the center of island D in Fig. 1(d) is localized near the outer turning point which is used to define the initial value of the angle as $\theta\simeq\pi$. In the presence of two superposed trains of pulses [Eq. (4)], the Kepler orbit bifurcates into segments of two Kepler orbits. During the time intervals $jT'+\tau<t<(j+1)T'$ the electron stays on the same Kepler orbit with action $n=n_{A_1}$ while it jumps onto an orbit with a larger action $n=n_{A_2}$ during the time intervals $jT'<t<jT'+\tau$. Immediately before the kicks at $t=jT'$, the periodic orbit [center of island B in Fig. 1(b)] has an angle $\theta(\tau)=\pi-(\pi/T_{n_{A_1}})\tau$. In the limit $\tau=T\simeq T_{n_{A_1}}/2$ the angle converges to $\theta\simeq\pi/2$ associated with the center of the period-2 island A_1 [Fig. 1(a)]. Variation of the delay time τ between the superposed pulses therefore allows control of the stroboscopic value of the angle θ (taken at the time of the kick). This protocol works equally well when τ takes negative values. In this case the angle θ increases with τ and converges to $\theta\simeq 3\pi/2$ as the wave packet is transported to the other period-2 island A_2. A negative chirp of τ is equivalent to interchanging of the role of the first and the second kicks within a pair, i.e., it corresponds to a different time at which the stroboscopic image is taken.

Figure 5 illustrates the level of control of the final angle of the Kepler orbit at the center of the wave packet that can

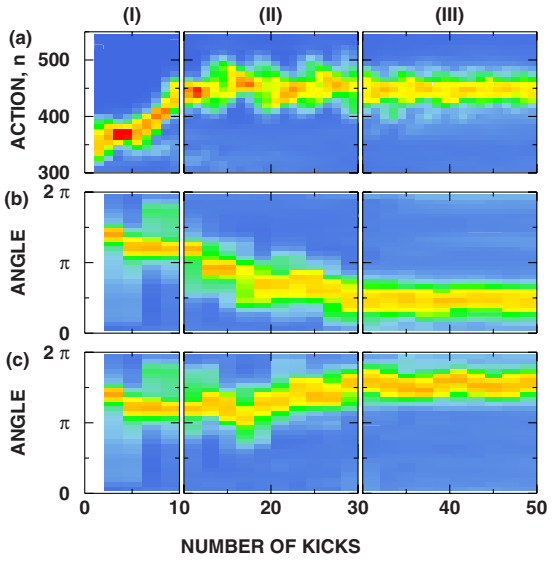

FIG. 5. (Color online) Calculated evolution of the distributions of (a) the principal action n and (b) and (c) its conjugate angle θ, during the HCP sequence (see text). A positive (negative) chirp in the time shift τ is used to steer the wave packet toward island A_1 (b) [island A_2 (c)]. The stroboscopic values in (b) and (c) are displayed for every other pulse in the superposed train F_s [Eq. (4)].

be achieved by the present protocol. The initial wave packet with principal action $n_i \sim 350$ is loaded slightly off the center of the main island so its initial angle is $\theta \sim 1.4\pi$. As the frequency of the train is chirped during the first ten pulses, $N=1-10$ (time interval I) the action [Fig. 5(a)] increases to $n \sim 450$. Following superposition of the second HCP train ($N>10$, time interval II) the action remains nearly constant [Fig. 5(a)] while the canonical angle [Fig. 5(b)] changes steadily to a final value $\theta=\pi/2$ associated with the period-2 island A_1. Once chirping of the time shift τ ceases when it reaches $\tau=T$ (i.e., for $N>28$, time interval III), the angle remains fixed. The final mean angle of the wave packet can be controlled by stopping the chirp when τ reaches the appropriate value. Because there exists a one-to-one correlation between the final angle and the final average momentum, the final angle can be measured using a probe HCP. With a negative chirp of τ the wave packet can be steered toward the island A_2 and, correspondingly, to $\theta=3\pi/2$ [Fig. 5(c)].

IV. EXPERIMENTAL REALIZATION

The above protocol has been experimentally realized using techniques described elsewhere [4,16]. Potassium atoms are photoexcited in a weak dc field of $\sim 250\ \mu\mathrm{V\ cm^{-1}}$ (which defines the z axis) to a narrow range of the lowest-lying, quasi-1D redshifted states in the $n_i=350$ Stark manifold. The atoms are initially oriented along the $+z$ axis. They are then subject to the HCP sequence which was produced by using a combiner to superpose the output of the programmable pulse pattern generator (PPPG) with those of other fast pulse generators and applying the resulting wave form to a nearby electrode. The PPPG divides time into a series of bins and in each outputs a voltage of 0 or V. The bin width is set at $\delta T=0.67$ ns and the value of V is kept constant. The number of atoms that survive is determined by selective field ionization in which a slowly varying ramped electric field is applied to the atoms and the liberated electrons are detected.

Figure 6 shows the dependence of the measured survival probabilities on the strength and direction of the probe pulse [Fig. 6(a)], on the number of kicks in the HCP train [Fig. 6(b)], and on the time delay τ_{delay} between the end of the HCP train and the application of a probe pulse [Fig. 6(c)]. While behavior similar to that seen in Fig. 4 is observed, it is less dramatic. A number of factors might account for this. The results in Fig. 4 were derived using a mix of the extreme maximally polarized redshifted states in the Stark manifold which have an average scaled dipole moment $\langle d_0 \rangle \sim -1.5$. Although the laser frequency can, in principle, be tuned to excite these states, this is difficult because the associated oscillator strengths are very small. Also, the effective laser linewidth is broadened by beam divergence and Doppler effects to ~ 12 MHz and therefore overlaps a number of Stark states, many of which have larger oscillator strengths and can be more efficiently excited [20]. These are centered around

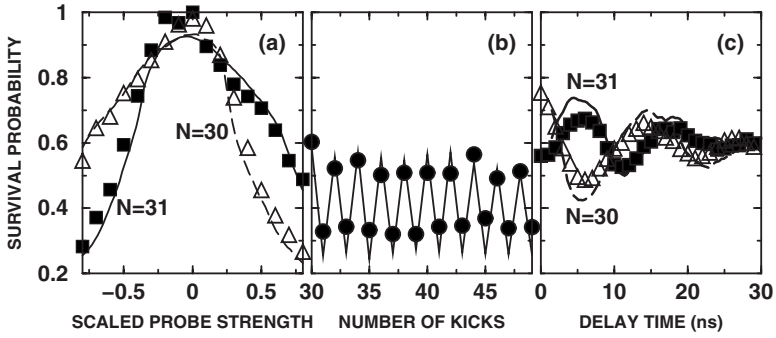

FIG. 6. Dependence of the measured and calculated survival probabilities on (a) the strength and direction of the probe kicks, (b) the number of kicks N in the HCP train, and (c) the delay time τ_{delay} between the end of the HCP train and application of a probe pulse. The parameters are the same as in Fig. 4. The open triangles show survival probabilities measured after the 30th kick, filled squares the 31st kick. Calculated survival probabilities after the 30th and 31st kicks are shown in (a) and (c) by dashed and solid lines, respectively. The initial wave packet used in the CTMC simulations is a mix of 36 Stark states with $n_i=350$, $m=0$ centered around $k=-175$ oriented along the same axis as the applied HCPs (see text).

$k \sim -291$ and have an average scaled dipole moment of $\langle d_0 \rangle \sim -1.25$. ^{39}K also has two ground state hyperfine levels, $4s(F=1)$ and $4s(F=2)$, that are shifted relative to one another by 462 MHz. Excitation from these levels gives rise to two different Rydberg series, i.e., two different excitation spectra. The present excitation wavelength is selected such that, in zero field, peaks from the two spectra overlap, leading to excitation of $n=350$ states from the $F=2$ level and (fewer) $n=347$ states from the $F=1$ level. Thus, given their similar Stark splittings in a field, the same mix of Stark states should be created for both. The potassium beam, however, also contains $\sim 7\%$ of ^{41}K. Depending on the size of the isotopic shifts, Stark states with even an opposite orientation of the average dipole moment might be created, which could significantly decrease the overall average dipole moment. Furthermore, while stray fields in the experimental region can be reduced to less than 50 μV cm^{-1} [4], their presence can lead to uncertainties in the magnitude and direction of the applied Stark field. These factors point to an average dipole moment somewhat below the value $\langle d_0 \rangle \sim -1.25$. Consistently good agreement between the experimental data and CTMC simulations is obtained, assuming an ensemble of initial states with an averaged scaled dipole moment of $\langle d_0 \rangle \sim -0.75$, i.e., with a mix of k values centered at $k \sim -175$. A reduced dipole moment leads to a less asymmetrical dependence of the survival probability on probe direction and strength following even and odd numbers N ($N>30$) of applied kicks [see Fig. 6(a)]. As expected, however, the asymmetry is reversed upon reversing the direction of the probe. As evident from Fig. 6(b), the predicted strong period-2 variations in survival probability are clearly seen. Little damping of these oscillations is evident with increasing N, indicating that a sizable fraction of the initial wave packet is transferred to, and remains trapped within, the period-2 islands. Furthermore, Fig. 6(c) shows that the time evolution of the final product state depends markedly on whether the pulse train contains an even or odd number of kicks, demonstrating that two different energy manifolds are indeed involved in the period-2 motion.

V. CONCLUSIONS

We have shown using a carefully tailored pulse sequence how wave packets can be transferred across the chaotic sea from a period-1 island to a period-2 island associated with the same periodic driving field. Moreover, we have shown that protocols can be devised to manipulate not only the principal action (or the principal quantum number) of a wave packet but also the stroboscopic value of the conjugate angle variable, even as the principal action is kept constant. The orientation and polarization of the initial state determine the efficiency of the protocol. However, even using the experimentally available initial state, the transfer can be observed, demonstrating the robustness of the present approach, which results from the near-adiabatic response of the dynamics to the lowest-frequency component in the pulse train.

The present protocol can also, in principle, be extended to transfer a wave packet onto a period-P stable island by using a superposition of P periodic trains of HCPs. In the limit of a large P, however, the periodic orbit becomes quite complex and involves many Kepler manifolds. Even a small deviation from the periodic orbit can cause the trajectory to diverge, meaning that the corresponding stable islands will be quite small or might even vanish. The success of the present classical description relies on the strong classical-quantum correspondence mediated by the large size of the stable island as compared to the quantum uncertainty $\hbar$. For period-P islands with $P \gg 1$, the island size can become smaller than this uncertainty. In this limit, the wave packet dynamics can depart from that of its classical counterpart, allowing a wave packet to remain localized despite residing, in part, in the chaotic sea. This phenomenon is termed quantum localization or quantum suppression of classical diffusion [21,22], and might become observable by extending the protocol described in this paper. In addition, P periodic trains of HCPs can be interpreted as P observations (projections) of the evolution of the Kepler orbit during one period T_n. Quantum localization is, in this context, caused by the freezing of the dynamics of the quantum system through frequent projections (the quantum Zeno effect [23]). Since such frequent projections suppress not only the intrinsic classical diffusion but also the effects of noise (or coupling to the environment), they have been suggested as a means to maintain coherence in quantum systems [24].

ACKNOWLEDGMENTS

S.Y. and J.B. acknowledge support by the FWF-SFB016 (Austria). C.O.R. acknowledges support by the OBES and U.S. DOE to ORNL, which is managed by the UT-Batelle LLC under Contract No. DE-4C05-00OR22725. Research at Rice is supported by the NSF under Grant No. PHY-0650732 and by the Robert A. Welch Foundation under Grant No. C-0734.

[1] H. Schuster, *Deterministic Chaos* (VHC, Weinheim, 1973).
[2] L. E. Reichl, *The Transition to Chaos: Conservative Classical Systems and Quantum Manifestations*, 2nd ed. (Springer, New York, 2004).
[3] P. M. Koch and K. A. H. van Leeuwen, Phys. Rep. **255**, 289 (1995).
[4] F. B. Dunning, J. C. Lancaster, C. O. Reinhold, S. Yoshida, and J. Burgdörfer, Adv. At., Mol., Opt. Phys. **52**, 49 (2005).
[5] D. A. Steck, W. H. Oskay, and M. G. Raizen, Science **293**, 274 (2001).
[6] J. Feist, A. Bäcker, R. Ketzmerick, S. Rotter, B. Huckestein, and J. Burgdörfer, Phys. Rev. Lett. **97**, 116804 (2006).
[7] A. Buchleitner, D. Delande, and J. Zakrzewski, Phys. Rep. **368**, 409 (2002).

[8] C. O. Reinhold, S. Yoshida, J. Burgdörfer, B. E. Tannian, C. L. Stokely, and F. B. Dunning, J. Phys. B **34**, L551 (2001).
[9] H. Maeda and T. F. Gallagher, Phys. Rev. Lett. **92**, 133004 (2004).
[10] S. Yoshida, C. O. Reinhold, P. Kristöfel, J. Burgdörfer, S. Watanabe, and F. B. Dunning, Phys. Rev. A **59**, R4121 (1999).
[11] M. Kalinski and J. H. Eberly, Opt. Express **1**, 216 (1997).
[12] S. Yoshida, C. O. Reinhold, E. Persson, J. Burgdörfer, and F. B. Dunning, J. Phys. B **38**, S209 (2005); S. Yoshida, C. O. Reinhold, E. Persson, J. Burgdörfer, B. E. Tannian, C. L. Stokely, and F. B. Dunning, Phys. Scr., T **110**, 424 (2004).
[13] H. Maeda, D. V. L. Norum, and T. F. Gallagher, Science **307**, 1757 (2005).
[14] J. J. Mestayer, W. Zhao, J. C. Lancaster, F. B. Dunning, C. O. Reinhold, S. Yoshida, and J. Burgdörfer Phys. Rev. Lett. **99**, 183003 (2007).
[15] M. Born, *The Mechanics of the Atom* (G. Bell and Sons, London, 1927).
[16] W. Zhao, J. J. Mestayer, J. C. Lancaster, F. B. Dunning, C. O. Reinhold, S. Yoshida, and J. Burgdörfer, Phys. Rev. Lett. **97**, 253003 (2006).
[17] T. Brabec and F. Krausz, Rev. Mod. Phys. **72**, 545 (2000).
[18] E. Persson, S. Fürthauer, S. Wimberger, and J. Burgdörfer, Phys. Rev. A **74**, 053417 (2006).
[19] J. Murray-Krezan and R. R. Jones, Phys. Rev. A **75**, 063411 (2007).
[20] C. L. Stokely, J. C. Lancaster, F. B. Dunning, D. G. Arbo, C. O. Reinhold, and J. Burgdörfer, Phys. Rev. A **67**, 013403 (2003).
[21] S. Yoshida, C. O. Reinhold, and J. Burgdörfer, Phys. Rev. Lett. **84**, 2602 (2000).
[22] E. Persson, S. Yoshida, X.-M. Tong, C. O. Reinhold, and J. Burgdörfer, Phys. Rev. A **66**, 043407 (2002).
[23] B. Misra and E. C. G. Sudarshan, J. Math. Phys. **18**, 756 (1977).
[24] L. Viola and S. Lloyd, Phys. Rev. A **58**, 2733 (1998).